Journal of Biomedical Optics

SPIEDigitalLibrary.org/jbo

Confocal microscopy to guide Erbium: yttrium aluminum garnet laser ablation of basal cell carcinoma: an *ex vivo* feasibility study

Heidy Sierra
Bjorg A. Larson
Chih-Shan Jason Chen
Milind Rajadhyaksha

SPIE

Confocal microscopy to guide Erbium:yttrium aluminum garnet laser ablation of basal cell carcinoma: an *ex vivo* feasibility study

Heidy Sierra,[*] Bjorg A. Larson,[*†] Chih-Shan Jason Chen,[‡] and Milind Rajadhyaksha[‡]
Memorial Sloan Kettering Cancer Center, Dermatology Service, 160 East 53rd Street, New York, New York 07940

Abstract. For the removal of superficial and nodular basal cell carcinomas (BCCs), laser ablation provides certain advantages relative to other treatment modalities. However, efficacy and reliability tend to be variable because tissue is vaporized such that none is available for subsequent histopathological examination for residual BCC (and to confirm complete removal of tumor). Intra-operative reflectance confocal microscopy (RCM) may provide a means to detect residual tumor directly on the patient and guide ablation. However, optimization of ablation parameters will be necessary to control collateral thermal damage and preserve sufficient viability in the underlying layer of tissue, so as to subsequently allow labeling of nuclear morphology with a contrast agent and imaging of residual BCC. We report the results of a preliminary study of two key parameters (fluence, number of passes) vis-à-vis the feasibility of labeling and RCM imaging in human skin *ex vivo*, following ablation with an erbium:yttrium aluminum garnet laser. [DOI: 10.1117/1.JBO.18.9.095001]

Keywords: laser ablation; basal cell carcinoma; confocal microscopy.

Paper 130542LR received Jul. 30, 2013; revised manuscript received Aug. 28, 2013; accepted for publication Aug. 29, 2013; published online Sep. 17, 2013.

1 Introduction

About 3.5 million new cases of nonmelanoma skin cancers are diagnosed in the USA every year,[1] and the incidence rate is increasing in other parts of the world, as well.[2] Of these cases, about 70% are basal cell carcinomas (BCCs). Surgical interventions such as Mohs surgery, excision, and electric desiccation and curettage are the commonly used modalities for treatment. Other modalities such as topical therapy, cryotherapy, photodynamic therapy, radiotherapy, and ablative and vascular laser treatments are used as less invasive alternatives.[3–5]

Laser treatment is suitable for certain types of patients such as those who may have multiple BCCs due to underlying hereditary disorders, excessive sun exposure or long-term immunosuppression, or those who may not tolerate surgical procedures, or those who may have low tolerance for the inflammatory side effects of topical therapies.[5–8] Laser ablation, e.g., is effective for treating superficial and nodular BCCs.[9–11] The treatment is relatively quick and convenient to perform in a single patient visit, and is minimally invasive, with finely controlled micrometer-level removal of tissue, reduced bleeding, scarring and infection, quicker recovery, and better cosmetic outcome. However, efficacy and reliability tend to be variable because the tissue is vaporized such that none is available for subsequent histopathological examination for residual BCC. Histopathologic examination is necessary and usually performed to confirm complete removal of tumor. (For example, during Mohs surgery, the BCC is removed in stages and the excision at each stage is examined for residual tumor by frozen histopathology. The presence and location of residual tumor guide the excision during the subsequent stage. This process of excision in stages continues until the histopathology indicates complete removal of tumor.) For laser ablation, this limitation may be addressed with high-resolution optical imaging that may detect BCC tumor directly on the patient.

Reflectance confocal microscopy (RCM), with its ability to image nuclear-level morphology, offers a possible approach. RCM imaging has shown the ability to detect BCCs *in vivo* with sensitivity of 92% to 100% and specificity of 97% to 88%,[12,13] and residual BCC in shave-biopsy wounds and Mohs surgical wounds on patients.[14–17] Hence, confocal imaging of residual BCC directly on the patient may provide a means to improve efficacy and reliability and guide laser ablation. However, laser ablation produces collateral thermal damage in the underlying layer of tissue. Thus, an optimization of ablation parameters will be necessary to control the damage and preserve sufficient viability in the underlying tissue, so as to subsequently allow labeling of nuclear morphology with a contrast agent and imaging of residual BCC. In this article, we report the results of a preliminary study of two key parameters (fluence, number of passes) vis-à-vis the feasibility of labeling and RCM imaging in human skin *ex vivo*, following ablation with an erbium:yttrium aluminum garnet laser (Er:YAG).

2 Materials and Methods

For this study, an IRB approved protocol (08-006, Procurement of discarded human skin specimens for research projects in Dermatology) allowed us to collect discarded tissue from

*These authors contributed equally as first authors.
†Current affiliation: Drew University, Department of Physics, 36 Madison Avenue, Madison, New Jersey.
‡These authors contributed equally as senior authors.

Address all correspondence to: Heidy Sierra, Memorial Sloan Kettering Cancer Center, Dermatology Service, 160 East 53rd Street, New York, New York 07940. Tel: +1-212-610-0826; Fax: +1-212-308-0739; E-mail: sierragh@mskcc.org

Mohs surgery. The discarded tissue consisted of either normal skin or BCCs. For ablation of superficial and nodular BCCs, our Mohs surgeon (coauthor CJC) uses an Er:YAG laser (Sciton Profile, Palo Alto, CA).

The Er:YAG laser operates at a wavelength of 2.94 μm, for which the absorption coefficient of water in tissue is $\sim$10,000 cm^{-1} such that the nominal thermal relaxation time is on the order of $\sim$1 μs in skin and nominal optical penetration depth is $\sim$1 μm.[18,19] In principle, when the laser operates with a pulse duration that is less than the thermal relaxation time, the ablation is spatially confined to within the optical penetration depth with no (or minimal) collateral thermal damage. In practice, thermally induced decrease in absorption coefficient, due to desiccation of uppermost layers of tissue with increase in fluence, results in longer thermal relaxation times and increased collateral damage in the underlying tissue.[19–21] The depth of damage has been observed to be $\sim$2 to 10 μm with pulses of durations 90 ns and 1 μs (with weak dependence on fluence).[22,23] The Er:YAG laser used for this study operates with pulses of duration $\sim$250 μs. For this pulse duration, reported depth of damage is on the order of $\sim$20 μm.[23,24] We used fluences in the range of 6.3 to 25 J/cm^2. The ablation spot was 4 mm in diameter.

Laser fluence, or energy per area, determines the depth of ablation. The nominal ablation threshold in skin is $\sim$1.6 J/cm^2. For each unit (1 J/cm^2) of fluence above the ablation threshold, $\sim$2.5 to 5 μm of tissue are removed per laser pulse.[22,23] To determine the effect of fluence on ablation depth for our laser, four fluence levels were chosen: 6.3, 12.5, 17.5, and 25 J/cm^2. These levels are routinely used by Mohs surgeons. Four pieces of discarded normal skin were ablated using each of the four levels, and vertical histology sections were prepared from each. The depth of ablation was measured at the shallowest and deepest regions, relative to the top surface (stratum corneum) of the adjacent nonablated skin, and reported as the observed range in the four pieces.

For imaging of residual BCC in ablated tissue, acetic acid was used for contrast. Acetic acid condenses chromatin which increases backscatter from the nuclei, causing the nuclear morphology to appear bright (known as acetowhitening), which then enhances the contrast and detectability of BCCs in reflectance confocal images.[25] Initially, discarded Mohs tissue (containing BCC) was immersed in 5% acetic acid for 30 s and preablation imaging was performed. For imaging, we used a clinical confocal microscope [Vivascope 1500, Caliber Imaging and Diagnostics (formerly, Lucid Inc., Rochester)], with 830-nm illumination and a 30×, 0.9 numerical aperture gel immersion objective lens. The optical sectioning is 2 μm and lateral resolution 0.7 μm. The field of view is 0.5 mm. Mosaicking of 16 × 16 images increases the field of view to 8 × 8 mm^2, which allows for observation of larger areas of tissue. A more detailed description of the acetowhitening protocol, tissue mounting, and imaging and mosaicking process can be found in previous papers.[25,26] Acquisition of images and mosaics was performed for pre and postablation.

The above-stated range of fluences was tested for feasibility of imaging nuclear morphology and detecting residual BCC after ablation. We ablated four pieces of tissues for each case, using a single pass (pulse). Furthermore, we tested for the highest fluence of 25 J/cm^2 with increased number of passes. Mohs surgeons use this approach for more aggressive ablations when the BCCs are deeper in the skin. A single pass with 25 J/cm^2 removes $\sim$100 to 120 μm of tissue. To investigate the feasibility for visualizing nuclear morphology and residual BCC when ablation is deeper, three pieces of tissues were imaged each, pre and postablation after two, three, and five passes. In all cases, the ablated tissue was again immersed in acetic acid and imaged. *En face* hematoxylin- and eosin-stained histology sections were prepared after ablation for comparison with confocal mosaics.

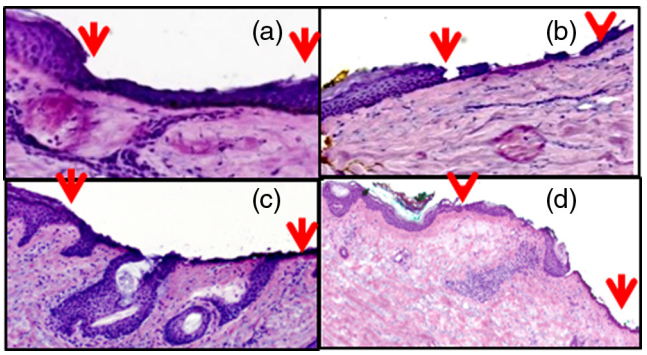

Fig. 1 Fluence determines ablation depth (ablated region is shown enclosed between red arrows): (a) A single pass (pulse) with fluence of 6.3 J/cm^2 ablates between $\sim$5 and 10 μm of tissue, (b) 12.5 J/cm^2 ablates between $\sim$50 and 80 μm, (c) 17.5 J/cm^2 ablates between $\sim$80 and 100 μm, and (d) 25 J/cm^2 ablates between $\sim$100 and 120 μm. With 17.5 and 25 J/cm^2, a thin line of dessicated tissue was observed on the ablated surface.

3 Results and Discussion

Figure 1 shows the histopathology of ablated tissue, in which the ablated regions are delimited by the red arrows. With a single pass (pulse) at the lowest fluence level of 6.3 J/cm^2, only part of the stratum corneum was removed, or between $\sim$5 and 10 μm of tissue. With 12.5 J/cm^2, the entire stratum corneum and part of the epidermis were removed, or between $\sim$50 and 80 μm of tissue. With 17.5 J/cm^2, most of the epidermis was removed, or between $\sim$80 and 100 μm of tissue. With 25 J/cm^2, the epidermis and part of the papillary dermis was removed, or between $\sim$100 and 120 μm of tissue. With 17.5 and 25 J/cm^2, a thin line of dessicated tissue was observed on the ablated surface.

Figure 2 shows an example of preablation and post ablation confocal mosaics and postablation *en face* histology. Figure 2(a) shows the preablation mosaic, where large BCC tumors are visible at the center, left, and along the right side of the tissue (red arrows). Figure 2(d) shows a magnified view, where nuclear morphology is more clearly seen in bright contrast, consistent with our expectation from the previous studies.[25,26] Figure 2(b) shows the postablation mosaic, where the two 4-mm spots of ablation are seen in the upper right and in the lower left regions. The red arrows indicate the locations of residual BCC tumor. The first ablation (lower left) was four passes with a fluence of 6.3 J/cm^2, to give a total fluence of 25 J/cm^2. The second ablation (upper right) was a single pass with a fluence of 25 J/cm^2. Each spot was thus treated with the same total fluence, but the two ablations represent the typical range used by Mohs surgeons, from lowest fluence and gentlest approach to highest and aggressive.

Figure 2(d) shows part [inset region in Fig. 2(a)] of the preablation tumor at higher magnification, showing nodular BCC in the upper right region of the tissue. The corresponding postablation region is shown in Fig. 2(e), following a single pass

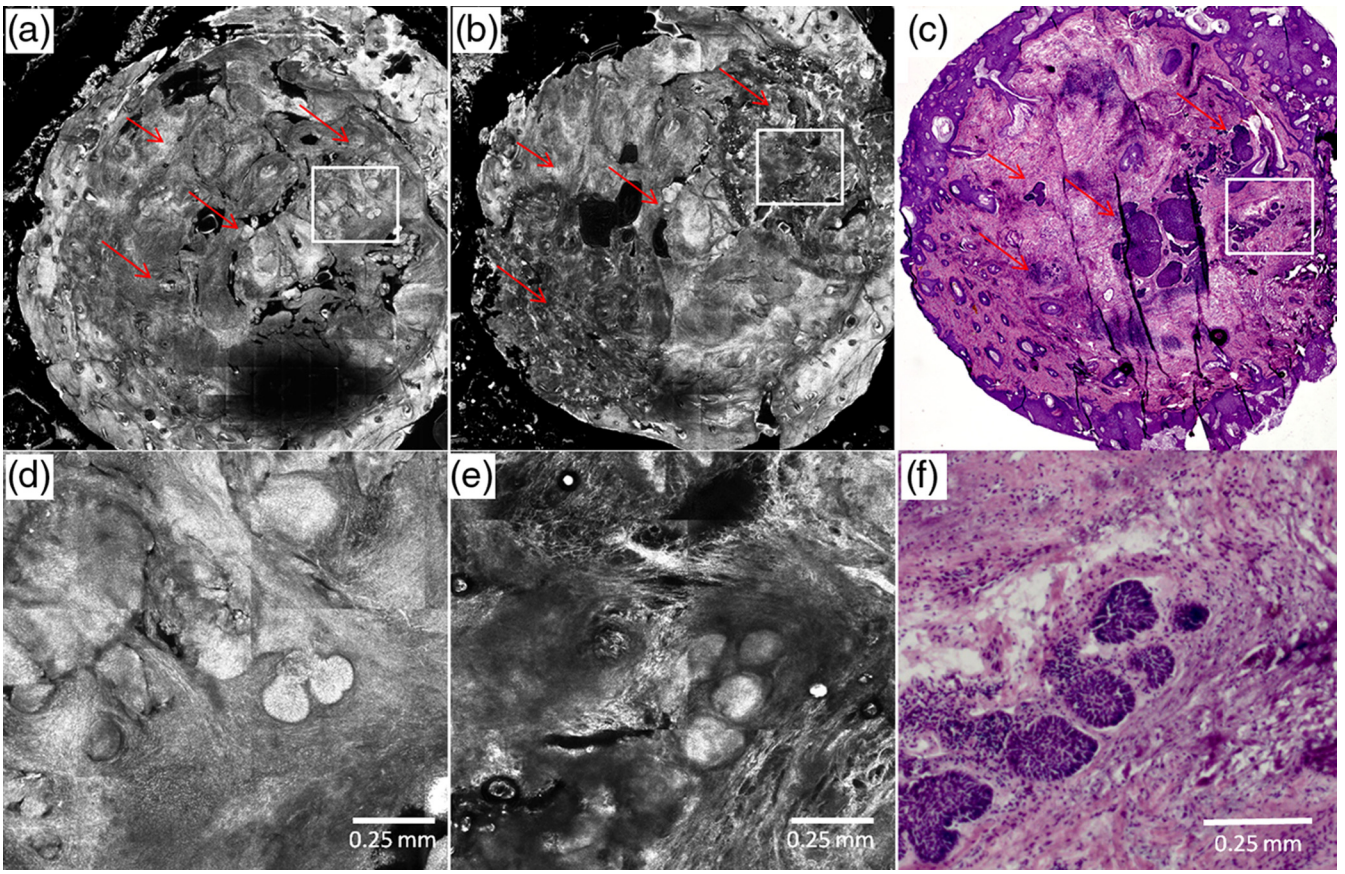

Fig. 2 Preablation (a) and postablation (b) confocal mosaics of discarded Mohs tissue, and *en face* hematoxylin and eosin-stained histology section postablation (c). The red arrows indicate the location of BCC tumor. The presence and location of residual BCC tumor in the postablation mosaic is confirmed by the histology. There are two ablation spots. The spot on upper right was treated with a single pass with 25 J/cm^2, and the lower left four passes with 6.3 J/cm^2. Each spot was thus treated with the same total fluence. Shown in (d) is a magnified view of inset region in (a), showing preablation bright nuclear morphologic detail of nodular BCC. Shown in (e) is a magnified view of the inset region in (b), showing postablation nuclear morphologic detail of residual BCC. Shown in (f) is a magnified view of the inset region in (c), showing the corresponding postablation residual BCC in the histology.

with 25 J/cm^2. Nuclear morphology is visualized in the postablated tissue in confocal images. The expected depth of ablation was ~100 to 120 μm. The BCC was not completely removed, and residual tumor was observed in the postablation mosaic. Figure 2(f) shows an *en face* histology of the same region after ablation, which clearly shows the residual tumor, similar to that seen in the confocal mosaic. The presence of residual BCC tumor in the mosaics was thus confirmed by the histology.

Following more aggressive ablations (which Mohs surgeons may use to treat deeper tumors), with two, three, and five passes with the highest fluence of 25 J/cm^2 (i.e.,total fluence of 50, 75, and 125 J/cm^2, respectively), postablation confocal mosaics showed that nuclear morphology can be imaged and residual BCC tumor can be distinguished from the normal tissue.

Figure 3 shows the postablated confocal mosaics after five passes with 25 J/cm^2, for a total fluence of 125 J/cm^2 [Fig. 3(a)]. Figure 3(d) shows the corresponding *en face* histology after ablation. The presence and location of residual BCC tumor in the mosaic are confirmed by the histology. This BCC is of the nodular type. Figure 3(b) shows a magnified view of the inset area in Fig. 3(a), clearly showing a bright cluster of nuclei in one of the residual nodules. This is confirmed in the corresponding histology in Fig. 3(e). Figure 3(c) shows a highly magnified view, along with the corresponding histology in Fig. 3(f), showing more clearly the nuclear morphology that is imaged in ablated tissue. This shows that nuclear morphology and residual BCC tumor can be detected after aggressively ablating deeper than ~120 μm into tissue. Furthermore, the morphology of the epidermis and surrounding dermis in the images was observed to appear similar to that seen in the histology.

In summary, we have shown that it is feasible to label nuclear morphology with a contrast agent and detect residual BCC in postablated tissue with RCM imaging. The results illustrate the potential of confocal imaging to guide laser ablation of BCCs. This investigation is the initial opening into a long-term study that will involve a number of technical developments: optimization of ablation parameters (fluence, number of passes, choice of laser, and wavelength) for minimal thermal damage, an effective contrast agent for use on patients (for example, aluminum chloride in reflectance or methylene blue in fluorescence), and optimization of labeling parameters (concentration, time) especially for the detection of tiny and sparse residual tumors. Alternatively, autofluorescence imaging modalities may be developed to avoid the use of endogenous contrast agents. Improvements to instrumentation may require the design of a small confocal microscope with controlled approach for

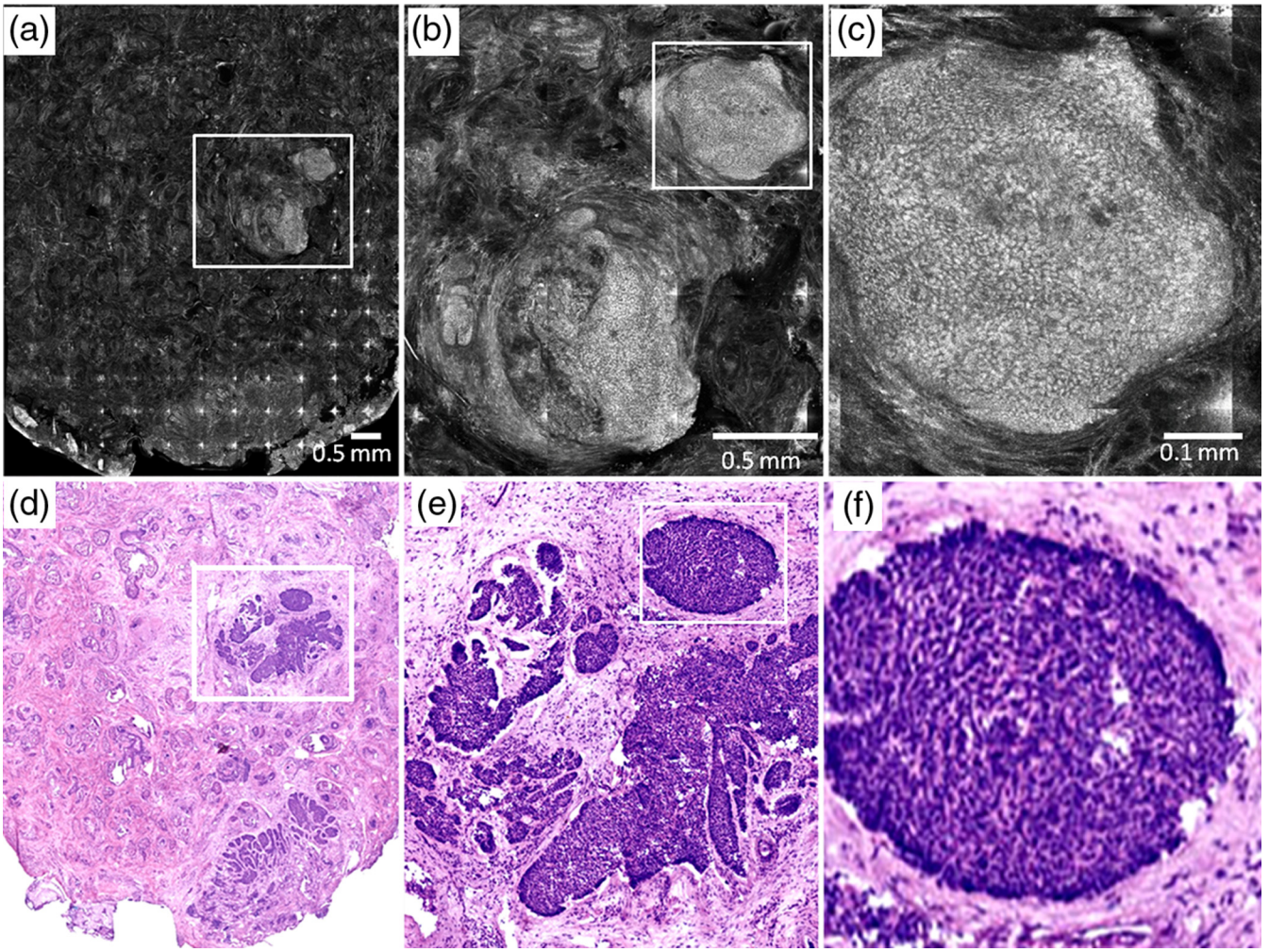

Fig. 3 Postablation confocal mosaic of discarded Mohs tissue, following five passes with fluence of 25 J/cm^2, showing (a) residual BCC tumor, (b) magnified view of the inset in (a), showing the residual tumor to be of nodular type, and (c) further magnified view of the inset in (b), clearly showing nuclear morphologic detail in the nodule. The corresponding *en face* histology (d) of the postablated tissue confirms the presence and location of tumor. Shown in (e) is a magnified view of inset region in (d), displaying clearly the tumor details including nuclear morphology. Shown in (f) is a magnified view of the inset region in (e), displaying more clearly the nuclear morphology, which confirms that (c) observed in the confocal image. This shows that nuclear morphology can be detected in confocal images after aggressively ablating deeper than 120 μm into tissue.

rapidly imaging over large areas of tissue in ablated wounds (for example, by mosaicking on the patient) and development of a cost-effective laser for clinical acceptance.

Regarding endogenous autofluorescence, an interesting study was recently published by Wang et al., demonstrating the possibility of imaging as well as the integration of imaging and ablation in skin, with a two-photon microscopy–based approach.[27] The short pulse duration of a femtosecond laser results in highly selective two-photon absorption and ablation in the focal plane. This may be useful for targeting very small microscopic types of BCC tumor, such micronodular, infiltrative, and sclerosing, with high specificity. For ablating larger tumors such as superficial and nodular BCCs, which are typically ten to hundreds of micrometers in both lateral extent and thickness, the high selectivity may not be necessary (and will require longer times to treat). In such cases, the relatively lower selectivity of the Er:YAG laser, along with relatively quicker treatment, may be sufficient for clinical utility. Of course, the approach of Wang et al. offers the important advantage of combining ablation and imaging into a single microscope.

Beyond such technical developments (both the development of Wang et al. and ours), clinical studies will involve testing for patient tolerance and variability of response to the optimal range of ablation parameters, efficacy of ablation and tumor recurrence relative to the standard of care (Mohs surgery, surgical excision), and analysis of cost benefits.

The focus of this study is on laser ablation, but this imaging approach appears to offer wider applicability. For example, we are currently developing RCM for imaging of residual BCCs on patients during Mohs surgery. Our preliminary results are promising and confirm the initial feasibility that was originally shown by Tannous et al.[16] Similarly, others have shown feasibility for RCM imaging to guide topical Imiquimod therapy and photodynamic therapy,[28,29] Thus, confocal imaging-based approaches may be useful for guiding laser ablation as well as some of the other modalities during the treatment of BCCs.

Acknowledgments

We thank the NIH for funding support (Grant R01EB012466), Mr. Steven Wilson and Mr. Reza Afzalneia for preparing frozen histology, and Dr. Kivanc Kose for providing technical

assistance with image stitching to generate the mosaics presented in this work.

References

1. H. W. Rogers et al., "Incidence estimate of nonmelanoma skin cancer in the United States, 2006," *Arch. Dermatol.* **146**(3), 283–287 (2010).
2. A. Lomas, J. Leonardi-Bee, and F. Bath-Hextall, "A systematic review of worldwide incidence of nonmelanoma skin cancer," *Br. J. Dermatol.* **166**(5), 1069–1080 (2012).
3. S. Amini et al., "Nonsurgical Innovations in the treatment of nonmelanoma skin cancer," *J. Clin. Aesthetic* **3**(6), 20–34 (2010).
4. L. Brightman et al., "Do lasers or topicals really work for nonmelanoma skin cancers?," *Semin. Cutaneous Med. Surg.* **30**(1), 14–25 (2011).
5. S. Choudhary et al., "Lasers in the treatment of nonmelanoma skin cancer," *Dermatol. Surg.* **37**(4), 409–425 (2011).
6. N. Konnikov et al., "Pulsed dye laser as a novel non-surgical treatment for basal cell carcinomas: response and follow up 12–21 months after treatment," *Lasers Surg. Med.* **43**(2), 72–78 (2011).
7. O. A. Ibrahimi et al., "755 nm alexandrite laser for the reduction of tumor burden in basal cell nevus syndrome," *Lasers Surg. Med.* **43**(2), 68–71 (2011).
8. C. J. Ballard et al., "The pulsed dye laser for the treatment of basal cell carcinoma," *Lasers Med. Sci.* **26**(5), 641–644 (2011).
9. R. Smucler and M. Vlk, "Combination of Er:YAG laser and photodynamic therapy in the treatment of nodular basal cell carcinoma," *Lasers Surg. Med.* **40**(2), 153–158 (2008).
10. R. Smucler et al., "Ultrasound guided ablative-laser assisted photodynamic therapy of basal cell carcinoma (US-aL-PDT)," *Photomed. Laser Surg.* **30**(4), 200–205 (2012).
11. S. Iyer et al., "Full face laser resurfacing: therapy and prophylaxis for actinic keratoses and non-melanoma skin cancer," *Lasers Surg. Med.* **34**(2), 114–119 (2004).
12. S. Nori et al., "Sensitivity and specificity of reflectance-mode confocal microscopy for in vivo diagnosis of basal cell carcinoma: a multicenter study," *J. Am. Acad. Dermatol.* **51**(6), 923–930 (2004).
13. P. Guitera et al., "In vivo confocal microscopy for diagnosis of melanoma and basal cell carcinoma using a two-step method: analysis of 710 consecutive clinically equivocal cases," *J. Invest. Dermatol.* **132**(10), 2386–2394 (2012).
14. A. Scope et al., "In vivo reflectance confocal microscopy of shave biopsy wounds: feasibility of intra-operative mapping of cancer margins," *Br. J. Dermatol.* **163**(6), 1218–1228 (2010).
15. D. E. Marra et al., "Detection of residual basal cell carcinoma by in vivo confocal microscopy," *Dermatol. Surg.* **31**(5), 538–541 (2005).
16. Z. Tannous, A. Torres, and S. González, "In vivo real-time confocal reflectance microscopy: a noninvasive guide for Mohs micrographic surgery facilitated by aluminum chloride, an excellent contrast enhancer," *Dermatol. Surg.* **29**(8), 839–846 (2003).
17. S. A. Webber et al., "Effectiveness and limitations of reflectance confocal microscopy in detecting persistence of basal cell carcinomas: a preliminary study," *Aust. J. Dermatol.* **52**(3), 179–185 (2011).
18. S. L. Jacques, "Role of tissue optics and pulse duration on tissue effects during high-power laser irradiation," *Appl. Opt.* **32**(13), 2447–2454 (1993).
19. J. T. Walsh and T. Deutsch, "Er:YAG laser ablation of tissue: measurement of ablation rates," *Lasers Surg. Med.* **9**(4), 327–337 (1989).
20. M. Perez, D. E. Bank, and D. Silvers, "Skin resurfacing of the face with the Erbium: YAG laser," *Dermatol. Surg.* **24**(6), 653–658 (1998).
21. K. Suthamjariya and R. R. Anderson, "Lasers in dermatology," Chap. 40 in *Biomedical Photonics Handbook*, T. Vo-Dinh, Ed., pp. 27–35, CRC Press, FL (2003).
22. U. Hohenleutner et al., "Fast and effective skin ablation with an Er:YAG laser: determination of ablation rates and thermal damage zones," *Lasers Surg. Med.* **20**(3), 242–247 (1997).
23. J. T. Walsh et al., "Er:YAG laser ablation of tissue: effect of pulse duration and tissue type on thermal damage," *Lasers Surg. Med.* **9**(4), 314–326 (1989).
24. M. Lukac1 et al., "Ablation and thermal depths in VSP Er:YAG laser skin resurfacing," *J. Laser Health Acad.* **2010**(10), 56–71 (2010).
25. Y. G. Patel et al., "Confocal reflectance mosaicing of basal cell carcinomas in Mohs surgical skin excisions," *J. Biomed. Opt.* **12**(3), 034027 (2007).
26. D. S. Gareau et al., "Confocal mosaicing microscopy in skin excisions: a demonstration of rapid surgical pathology," *J. Microsc.* **233**(1), 149–159 (2009).
27. H. Wang et al., "Imaging directed photothermolysis through two-photon absorption demonstrated on mouse skin—a potential novel tool for highly targeted skin treatment," *J. Biophotonics*, 1–8 (2013).
28. M. Ulrich, S. Lange-Asschenfeldt, and S. Gonzalez, "The use of reflectance confocal microscopy for monitoring response to therapy of skin malignancies," *Dermatol. Pract. Concept* **2**(2), 43–52 (2012).
29. M. Venturini et al., "Reflectance confocal microscopy allows in vivo real-time noninvasive assessment of the outcome of methyl amino laevulinate photodynamic therapy of basal cell carcinoma," *Br. Assoc. Dermatol.* **168**(1), 99–105 (2012).